


## Measuring the effects of a pulsed excitation on the buildup of acoustic streaming and the acoustic radiation force utilizing an optical tweezer

Christoph Goering \* and Jürg Dual 

*ETH Zurich, Institute for Mechanical Systems, Leonhardstr. 21, 8092 Zurich, Switzerland*

 (Received 24 December 2021; revised 27 April 2022; accepted 28 April 2022; published 13 May 2022)

Pulsed excitations of piezoelectric transducers affect during the buildup the force contributions from acoustic streaming (AS) and the acoustic radiation force (ARF) to the total force in a standing pressure wave differently. We find with an optical tweezer as measuring instrument that during the first 120 000 excitation periods and across different pulsing frequencies, the AS-induced displacement is on average less than 20% of its nonpulsed value for a duty cycle of 50%, whereas the ARF-induced displacement is around 50%. These findings show that a pulsed excitation can be a tool for reducing AS compared to the ARF.

DOI: [10.1103/PhysRevE.105.055103](https://doi.org/10.1103/PhysRevE.105.055103)

### I. INTRODUCTION

In acoustofluidic devices two main forces lead to a displacement of an immersed object within a pressure wave field: the drag force from acoustic streaming (AS) and the acoustic radiation force (ARF). AS typically arises due to viscous losses. These viscous losses can appear in the fluid itself (Eckart-type streaming) [1] or in a viscous boundary layer. This boundary layer can be either at the interface between the fluid cavity and the surrounding medium (Schlichting and Rayleigh streaming) [2,3] or even around the object itself (microstreaming) [4]. Apart from microstreaming, the occurrence of AS is independent of the immersed object properties.

The other main force is the ARF. As with AS, it is a second-order time-averaged effect and appears due to scattering of the acoustic incident field at the object surface [5–7]. In contrast to AS, the ARF depends also on the ratios of the object and fluid material. For example, an object of any material but with an acoustic contrast factor  $\Phi$  [6] of zero magnitude is not displaced due to the ARF because the ARF scales linearly with  $\Phi$ . However, this object will be displaced by the drag force arising from AS for any value of  $\Phi$ .

Besides the material influence, another important difference is the scaling with the object dimension for the limit of small particles compared to the acoustic wavelength [6,8]. On the one hand, the drag force from AS scales for a spherical object with the radius ( $F_{AS} \propto R$ ), and on the other hand, the ARF scales with the object volume ( $F_{ARF} \propto R^3$ ) [6]. At the critical radius ( $R = R_{crit}$ ) both forces are equal in magnitude ( $F_{ARF} = F_{AS}$ ). For a radius smaller than the critical radius ( $R < R_{crit}$ ) [6,9] the drag force from AS dominates over the ARF and vice versa. The forces from AS can be neglected if  $R \gg R_{crit}$ .

In many acoustofluidic applications the drag forces from AS are undesired because they can counteract the ARF [10,11] and hinder the application's desired function, e.g., the

trapping or focusing of particles. Therefore, different techniques for the suppression of AS have been investigated in recent years. Hoyos and Castro applied a pulsed excitation to the piezoelectric transducer (PZT) leading to a reduction of the steady-state streaming flow of up to 50% compared to the unpulsed flow [12,13]. Karlsen *et al.* [14] utilized in simulations and experiments inhomogeneities of the density and of the compressibility within the fluid to reduce AS. Bach and Bruus [15] optimized the shape of channels with numerical simulations to reduce AS by two orders of magnitudes while retaining the same level of acoustic pressure. The same AS suppression magnitude was achieved by Winkelmann and Bruus [16]. They investigated analytically and numerically the usage of acoustic electroosmosis to suppress AS.

The combination of optical tweezer (OT) and the acoustic trap is relatively new and rare. To the best of the authors' knowledge, in 2011 Thalhammer *et al.* [17] were the first to combine these two kinds of traps to measure the acoustic forces with the OT. In 2014, Bassindale *et al.* [18] utilized an holographic OT to measure acoustic forces in three dimensions, and Fury *et al.* [19] used the fine spatial optical resolution and the wide range of acoustic trapping for spatially precise manipulation of microbubbles. In 2015 and 2016 Lakämper *et al.* [20] and Lamprecht *et al.* [21] used our single-beam optical trap to measure the acoustic forces in two and three dimensions on silica microparticles. In 2016 Thalhammer *et al.* [22] also combined a holographic OT with an acoustic trap to measure the force for excitation frequencies above 20 MHz. Lastly, in 2021 Lamprecht *et al.* [23] used our setup to measure the resulting final rotational velocity on microparticles due to the acoustic viscous torque.

In 2021 we [24] used an OT setup to measure for the first time the buildup of the ARF and AS on a single spherical particle in a precisely characterized MHz pressure field. We found that the buildup of AS is much slower than the buildup of the ARF. Our measurements of the AS buildup revealed approximately 4 times longer buildup of AS than the theoretical prediction from the momentum diffusion time approximation [24,25]. Those experimental results indicated that the

\*goering@imes.mavt.ethz.ch

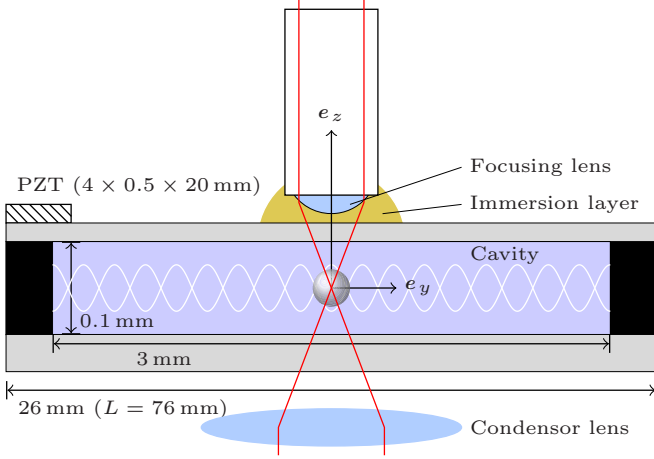


FIG. 1. Schematic of device and buildup measurement setup.

longer-than-expected AS buildup might be the reason for the pulsed excitation to successfully suppress AS [12,13].

Here we use our measurement routine, the OT setup, the acoustofluidic bulk acoustic wave device, and the same acoustic excitation frequency from [24] to dynamically measure the buildup of the ARF and AS for a acoustic excitation with various pulsing parameter settings.

## II. MEASUREMENT PROTOCOL

We will highlight the main points of the measurement protocol for the buildup measurements (BMs). A more extensive explanation of each step can be found in Goering and Dual [24]. We can measure with the OT the buildup of the ARF and AS separately because we determined our BM locations such that those two effects are orthogonal to each other; i.e., the ARF points in the direction of our  $y$  coordinate and the AS points along  $z$  (see Fig. 1). Our setup (see Figs. 2, 3, and 4) has in its back focal plane two quadrant photo detectors (QPDs) for detecting the movement in each spatial direction separately [20,21,23,24]. One QPD measures the information of the  $x$  and  $y$  coordinate, and the other QPD measures the  $z$  information. Hence, the buildup information of the ARF and AS is also separated in the data.

Our OT consists of a single laser with a maximal power of 200 mW and a wavelength of  $\lambda_L = 785$  nm (Omicron GmbH, Rodgau, Germany). The laser traps a spherical  $\text{SiO}_2$  particle with a radius of  $R = 1.03$   $\mu\text{m}$  (Microparticle GmbH, Berlin, Germany; the same as in [24]) and acts also as the light source for the displacement signal on the QPDs (see Fig. 4). The  $\text{SiO}_2$  particles have the advantage that they are hydrophilic, which makes handling with our OT easier. As shown in [24] the critical radius for our experimental settings is  $R_{\text{crit}} \approx 0.6$   $\mu\text{m}$ , which makes the movement of the used particles ARF dominated. Nevertheless, we can separate the AS- and ARF-induced movement because the effects are for our BM locations orthogonal to each other.

In the normal trapping mode it is not possible to measure the buildup of AS and the ARF because the time constant of the OT ( $\tau_{\text{OT}} \approx 1.59$  ms [24]) is much larger than the ones of interest ( $\tau_{\text{AS}} \approx 1.44$  ms and  $\tau_{\text{ARF}} \approx 1.4$   $\mu\text{s}$  [24]).  $\tau_{\text{ARF}}$  is

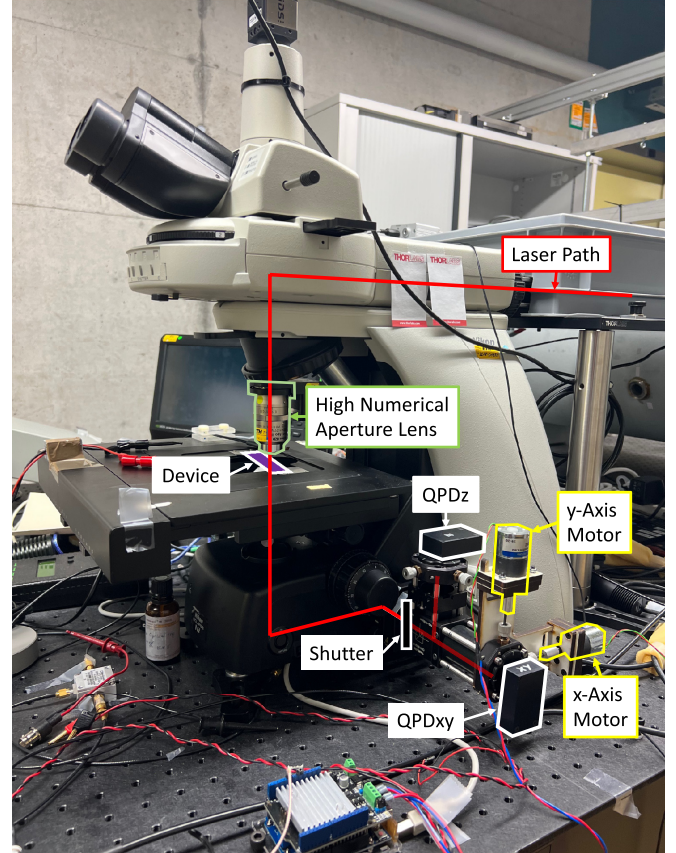


FIG. 2. Photograph of optical trapping setup with highlighted important equipment.

defined as the buildup time of the ARF, which is approximated by the buildup time  $\tau$  of a single degree of freedom acoustic resonance mode with quality factor  $Q \approx 40$  and  $\tau_{\text{AS}}$  is the momentum diffusion time [25]. Therefore, we need to switch the laser almost completely off such that the formerly stably trapped particle becomes free-floating. If the particle is free-floating, there is no influence from the OT characteristics on the BM.

For stable trapping of our particles the laser power must be greater than at least 75 mW. However, this laser intensity is too high for the QPDs in the back focal plane, and they would

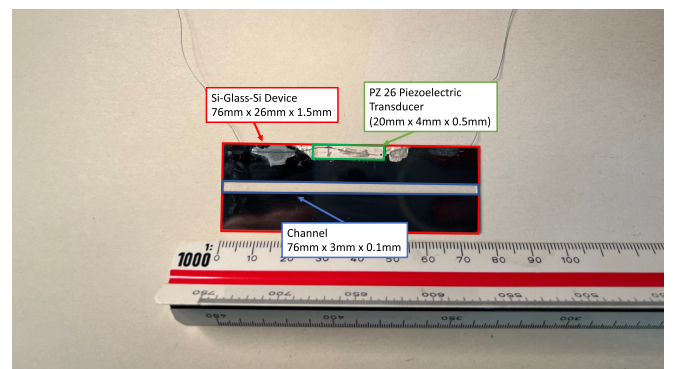


FIG. 3. Photograph of acoustofluidic device with highlighted parts.

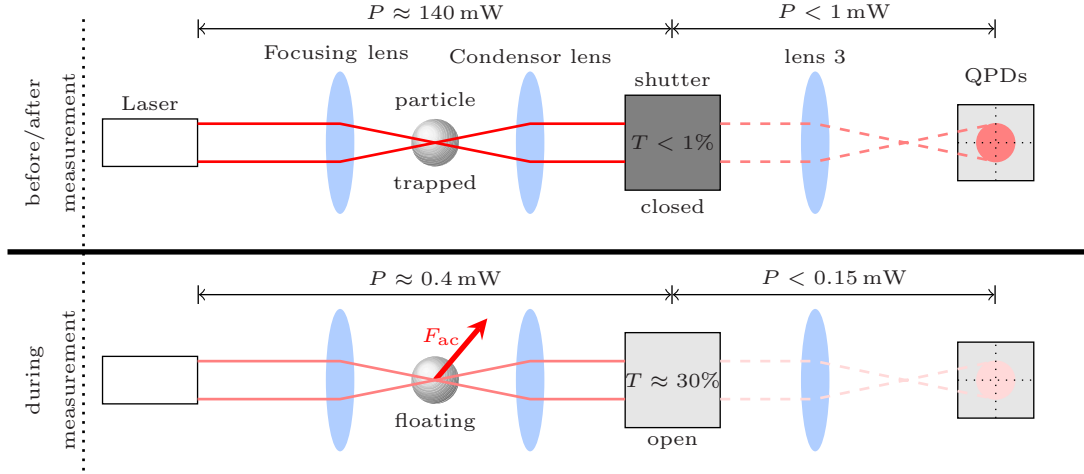


FIG. 4. Schematic of optical trapping setup, laser settings ( $P$ : laser power), and optical shutter settings ( $T$ : transmittance for  $\lambda_L = 785$  nm) before and after the buildup measurement (BM; top) and during the BM (bottom). During the BM the particle is free-floating, the laser power is reduced as low as possible, the shutter is opened to allow optical position detection on the quadrant photo detectors (QPDs), and the ultrasound is switched on; hence an acoustic force  $F_{ac}$  acts on the particle. Before and after the BM all states are switched to their respective opposite.

be damaged without further modifications. Therefore, an optical shutter (FOS NIR 1100, LC-TEC, Borlänge, Sweden) is installed in the laser path before the QPDs (see Fig. 4). The shutter transmittance  $T$  is proportional to the applied voltage of the shutter driving signal. In earlier experiments with our OT the optical shutter was implemented as a fixed set of neutral density filters that limited the transmitted intensity to less than 0.1% of the trapping intensity [20,21,23]. Before and after our BMs the particle is stably trapped.

One single BM follows the sketched process of Fig. 5 (see also Fig. 4). The particle is free-floating during the BM and retrapped at the end. The spot size of the OT is not finite, and retrapping to the exact same location unlikely. Therefore at the beginning of each BM the Python control software checks if the offset of the QPDs needs to be adjusted. A QPD with zero offset is in the middle of the linear regime between the displacement of the particle and the measured voltage at the QPDs. Hence, the offset adjustment before a new BM enables the quantitative comparison between BMs because

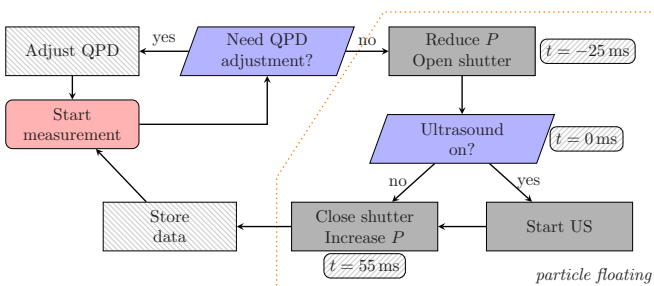


FIG. 5. Process diagram for one measurement cycle. The gray rectangles represent the processes during the buildup measurement (BM). During this time the particle is free-floating (orange area). All other process steps are before or after a BM. The time stamps in the hatched rounded rectangles represent the times when the process attached to them is executed. One measurement cycle takes about 2 s to be executed. The BM itself is less than 100  $\mu$ s.

all begin with the same offset. If an adjustment is necessary, an automated incremental offset change is performed and the QPD values are checked again. If there is no action needed, the laser changes its power  $P$  from 140 mW to 0.4 mW and the shutter starts to open. The laser power change takes effect in less than 3 ms, whereas the shutter is specified to open within 15 ms from fully closed to 90% of its fully open state. To ensure the shutter is maximally opened we wait another 10 ms before the ultrasound (US) is switched on. In this first 25 ms ( $t = -25$  ms to  $t = 0$  ms) the particle is free-floating and will therefore start sedimenting. We showed in [24] that the particle travels less than  $0.052 \mu\text{m} \approx 0.05 R$  in this time towards the bottom of the device. This distance is uncritical for the further BM. At  $t = 0$  ms the US is switched on for 30 ms. The particle is displaced due to the acoustic forces  $F_{ac}$ . At  $t = 55$  ms, the shutter starts closing and the laser power is increased to its starting power again to retrap the same free-floating particle. After the output of the data a new BM starts. The time between two consecutive BMs is more than 2 s. The data for one BM are collected over a timespan of 100 ms where the US is switched on for 30 ms only. The acoustic excitation frequency  $f_{ex}$  is set to the same value of 4.015 MHz where we measured 17 standing pressure nodal planes. With a maximal force amplitude of 1.25 pN for a  $4.39 \mu\text{m}$  diameter particle and a maximal force amplitude of 0.17 pN for a  $2.06 \mu\text{m}$  diameter particle (both measured with the OT [24]) and the assumption of a one-dimensional pressure wave the acoustic pressure [see Eqs. (30a) through (30c) in [6]] inside the fluid cavity is about 100 kPa [24]. With this short time of US excitation and the fast buildup constant for the ARF ( $\tau_{ARF} \approx 1.4 \mu\text{s}$ ) compared to the relatively long time between BMs, the system has the same starting conditions for each BM respectively.

One whole measurement series consists of six different  $\Delta y_i$  positions, one fixed pulse frequency  $f_p$ , and one fixed duty percentage. Per  $\Delta y_i$  we perform 75 BMs with acoustic excitation (*on BMs*) and 75 BMs without excitation (*off BMs*). As result for this combination of pulse frequency

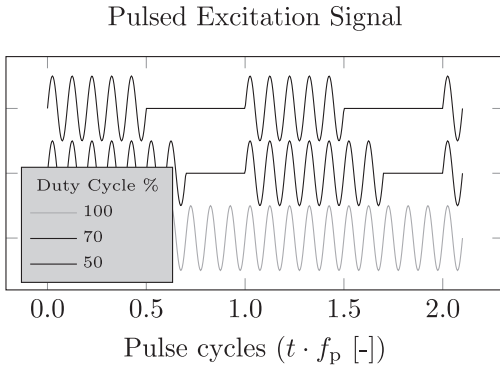


FIG. 6. Schematic of pulsed acoustic excitation for three different duty percentages (50%, 70%, and 100%) over pulsing cycles  $t f_p$  with the relation  $f_{\text{ex}} = k f_p$  (here  $k = 10$ ).

$f_p$ , position  $\Delta y_i$ , and duty percentage we take the difference of the averaged *on* BMs subtracted from the averaged *off* BMs ( $\Delta V_i = \text{avg.on} - \text{avg.off}$ ). While the BM is prepared, the first 25 ms are exactly the same between *on* and *off* BMs. The repetition per location  $\Delta y_i$  is necessary to reduce the unwanted noise from the Brownian motion. As in [24], we measure with a sampling frequency of 1.25 MHz and average the measured data over a centered window of  $80 \mu\text{s}$  (101 data points).

Our BMs locations within the standing pressure field are the same as in [24]. At those locations the forces from AS and the ARF itself were large enough in our device. All BMs are in the middle plane between the top and bottom fluid-device interface of our fluid cavity ( $\Delta z = 0 \mu\text{m}$ ). Undisturbed Rayleigh streaming would lead to no streaming velocity in the middle plane along  $e_z$ . However, the excitation in our device is from one side only, which leads to asymmetries in the AS field. These asymmetries result from the inclusion of the Stokes drift term in the numerical model as opposed to using a simplified limiting velocity approach for the AS calculation which does not include Stokes drift and leads to symmetrical streaming patterns while having an one-sided acoustic excitation [26]. We have shown in [24] with a two-dimensional numerical simulation where we model the device-cavity cross section as it is in the device that for our BM locations the streaming rolls can be over the whole channel height. Therefore, we can measure at  $\Delta z = 0 \mu\text{m}$  a streaming velocity in  $e_z$  direction.

All BMs for a certain pulse frequency  $f_p = f_{\text{ex}}/k$  were performed consecutively starting with a duty percentage of 100% and going down to 50% (see Fig. 6). Between the different pulse frequencies  $f_p$  the device was taken out of the OT setup, emptied, cleaned, and refilled. This procedure was necessary to ensure the same experimental conditions at the start and during the BMs because our device is a simple cavity with a [product-units = bracket-power] $3 \times 0.1$  cross section etched in silicon with two open sides of the cavity (see Fig. 1). This rather wide channel dimension is necessary because of the large half cone angle of the laser beam ( $\approx 72^\circ$ ). The channel walls are nontransparent for the laser wavelength, and hence a minimal distance must be kept from the channel walls to facilitate unhindered measurements.

To prevent evaporation of water during the experiments we seal both sides with a drop of silicone oil that is less likely to evaporate due to its higher viscosity. Nevertheless, at the end of one measurement series some water had left the channel. This change of water volume in the cavity is less than 5% of its overall volume. The evaporation occurs at the sides of the cavity and does not lead to air bubbles within the cavity.

The disadvantage from this procedure is the dis- and reconnecting of the electric cables to the PZT, as well as the application of a new immersion layer on top of the device for the oil immersion lens of our OT. We limited the difference in immersion layer volume and initial placement, as well as cable connection between two different pulse frequencies  $f_p$  to a minimum to ensure comparability between two different data sets. Nevertheless, there were small changes, and we adapted the voltage at the function generator between the different pulse frequencies to have the same acoustic pressure  $p_a$  in the cavity and hence the same magnitude of the ARF and AS. We did this by comparing and adjusting the time it takes until the particle displacement is outside of the linear regime of the QPDs. This is a manual process, and, hence, there are small differences in the experiments between different BM series.

The pulse frequencies  $f_p$  we chose such that the fraction  $f_{\text{ex}}/f_p$  is an integer  $k$ . This means that per pulsing cycle ( $T_p = 1/f_p$ )  $k$  excitation periods  $t_0 = 1/f_{\text{ex}}$  are within  $1 T_p$ . As integer we set  $k \in \{1000, 5000, 10000\}$ . The investigated duty percentages are 100%, 90%, 80%, 70%, 60%, and 50%. The percentage value reflects the relative time the excitation is switched on within  $1 T_p$  (see Fig. 6). The BM with 100% duty (*always on*) is the baseline where the excitation is on for the entire BM. This BM is used for normalizing all other duty percentages at the same point  $\Delta y_i$  and pulse frequency  $f_p$ . The shortest pulse duration is for  $k = 1000$  and 50% duty width. With these settings 500 *on* periods are followed by 500 *off* periods before starting over. The pressure amplitude buildup is proportional to  $\propto [1 - \exp(-t/\tau_{\text{ARF}})]$  for this linear oscillating system. After  $50/f_{\text{ex}} \approx 12.5 \mu\text{s}$  (50 excitation periods) the system is at 99.96% of its steady-state amplitude. Although our system is subjected to two frequencies ( $f_{\text{ex}}$  and  $f_p$ ), there are no influences on the pressure wave frequency because the buildup is much faster than the shortest pulse.

All in all, compared to [24] these three changes in the experimental settings are present: (1) 75 instead of 50 repetitions, (2) fixed  $\Delta z$  to  $0 \mu\text{m}$ , and (3) pulsed excitation signal.

### III. RESULTS AND DISCUSSION

Before discussing our results, we want to emphasize that our experiments are very sensitive to external disturbances as well as the experimental condition. Because the whole experiment was newly initialized between the different  $k$  values and, therefore, experimental conditions might change slightly, the results of different  $k$  values are not fully quantitatively comparable. However, the trend for different  $k$  values is nevertheless conclusive.

In Figs. 7, 8, and 9 the results of the BMs over time for  $\Delta y_i = -0.04 \text{ mm}$ ,  $\Delta y_i = -0.05 \text{ mm}$ , and  $\Delta y_i = -0.06 \text{ mm}$  are plotted, respectively. The figures consist of two columns (left for the ARF buildup and right for the AS buildup) and

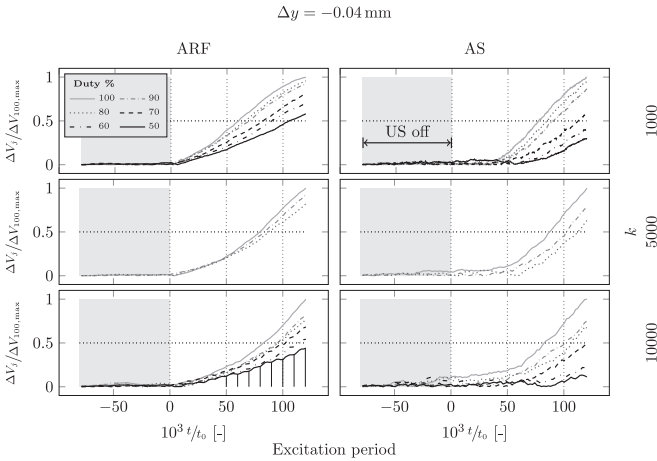


FIG. 7. Evolution of averaged voltage differences  $\Delta V_y$  (left column; ARF associated) and  $\Delta V_z$  (right column; AS associated) for three different pulsing frequencies  $f_p$  and different duty percentages at  $\Delta y = -0.4$  mm over excitation periods  $t/t_0$  with  $t_0 = 1/f_{ex}$ . For the first row  $f_p = f_{ex}/1000$ , for the second  $f_p = f_{ex}/5000$ , and for the last row  $f_p = f_{ex}/10000$ . The data per plot are normalized to the maximal amplitude of the data series with a duty percentage of 100%. The gray-shaded area of each plot marks the time when the US is off. Additionally, the vertical solid lines in the bottom left plot mark the beginning of a new pulsing cycle.

three rows for the three different pulsing frequencies  $f_p$ : in the first row  $f_p = f_{ex}/1000$ , in the second row  $f_p = f_{ex}/5000$ , and in the third row  $f_p = f_{ex}/10000$ , respectively. For  $f_p = f_{ex}/5000$  the data for the duty percentages of 70%, 60%, and 50% are not available. A data series with a duty percentage of 100% has the same experimental settings as the data from [24].

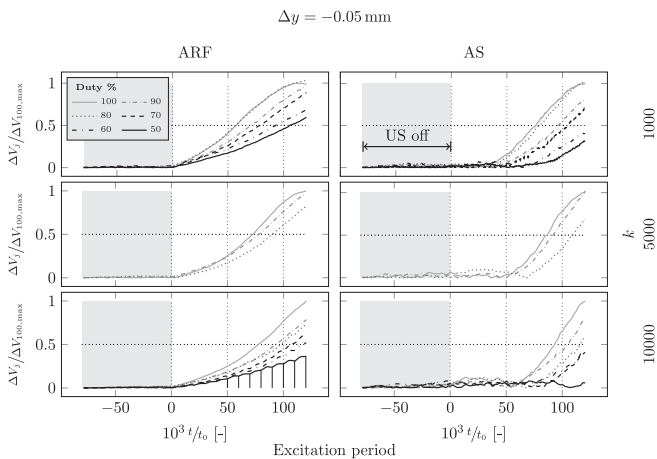


FIG. 8. Evolution of averaged voltage differences  $\Delta V_y$  (left column; ARF associated) and  $\Delta V_z$  (right column; AS associated) for three different pulsing frequencies  $f_p$  and different duty percentages at  $\Delta y = -0.5$  mm over excitation periods  $t/t_0$  with  $t_0 = 1/f_{ex}$ . For the first row  $f_p = f_{ex}/1000$ , for the second  $f_p = f_{ex}/5000$ , and for the last row  $f_p = f_{ex}/10000$ . The data per plot are normalized to the maximal amplitude of the data series with a duty percentage of 100%. The gray-shaded area of each plot marks the time when the US is off. Additionally, the vertical solid lines in the bottom left plot mark the beginning of a new pulsing cycle.

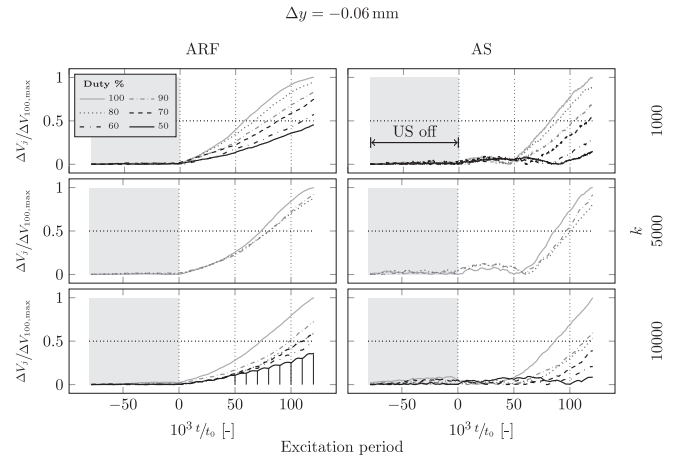


FIG. 9. Evolution of averaged voltage differences  $\Delta V_y$  (left column; ARF associated) and  $\Delta V_z$  (right column; AS associated) for three different pulsing frequencies  $f_p$  and different duty percentages at  $\Delta y = -0.6$  mm over excitation periods  $t/t_0$  with  $t_0 = 1/f_{ex}$ . For the first row  $f_p = f_{ex}/1000$ , for the second  $f_p = f_{ex}/5000$ , and for the last row  $f_p = f_{ex}/10000$ . The data per plot are normalized to the maximal amplitude of the data series with a duty percentage of 100%. The gray-shaded area of each plot marks the time when the US is off. Additionally, the vertical solid lines in the bottom left plot mark the beginning of a new pulsing cycle.

Hence, the results also show the same behavior: the initial buildup of the ARF is significantly faster than the buildup of AS. The data for  $k = 1000$  and 80% duty width show an unexpected behavior because the magnitude is almost as strong as for 100%. During the 80% BM series an unknown external disturbance caused a significant drop in the ambient room temperature (see also Fig. 10). The measurement itself is not very sensitive to temperature fluctuations within  $1^\circ\text{C}$ . However, the OT is very sensitive to ambient noise: e.g., fast movement of a person in the room or careless opening or closing of the door can be detected by the OT. We attribute this outlier of  $k = 1000$  and 80% to an external disturbance that also caused the significant temperature drop.

For the three different pulsing frequencies the time difference between the ARF and AS of the 100% duty width measurements for reaching 50% of the maximal value

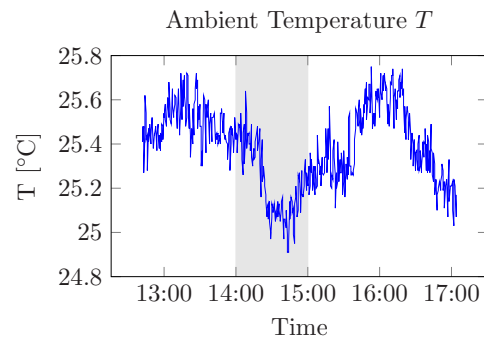


FIG. 10. Ambient temperature  $T$  at device for  $k = 1000$  BM series over time. The experiment of 80% occurred between 14:00 and 15:00 (gray-shaded area).

(horizontal dotted lines in Fig. 8) is  $76-57 = 19[\times 10^3 t/t_0]$ ,  $88-73 = 15[\times 10^3 t/t_0]$ , and  $94-78 = 16[\times 10^3 t/t_0]$  for  $k = 1000, 5000,$  and  $10\,000$ , respectively. This 50% criterion is the same measure we used in [24], and, in addition, the time differences of the ARF and AS have the same magnitudes. However, the time at which the ARF is over 50% of its maximal value is varying for the different  $k$  values. Even though we limited the changes of the experimental settings between measurement series to a minimum, there are slight differences in the amplitude of the incident acoustic pressure field which cause these different values of the 50% criteria. This is also the reason why for increasing values of  $k$  the start time of the AS-induced displacement is at a later point in time. The results for the three locations  $\Delta y_i = -0.4$  mm,  $\Delta y_i = -0.5$  mm, and  $\Delta y_i = -0.6$  mm show qualitatively and quantitatively the same behavior.

For all data series in all three plots, the normalized data are zero for  $t/t_0 = t/f_{\text{ex}} < 0$  (gray-shaded area). This is the time span where the US excitation is not switched on yet. Since the difference of the averaged on data subtracted from the averaged off data is shown and since both have the exact same protocol before the US is switched on, this behavior is expected and serves as quality control of a data series. A value close to zero after  $t > 0$  indicates that there is no difference in the movement of the particle along this direction for a switched-on US and a switched-off US. When the US is switched off, just gravity and the opposite directed buoyancy force are acting on the particle because the trapping laser is reduced to such a low laser power that the trap exerts negligible forces on the particle.

In addition, for a pulse frequency of  $f_p = f_{\text{ex}}/10\,000$  and a duty cycle of 50% the times where the US is switched on and off are visible in the data for the ARF (see bottom left plots in Figs. 7 to 9). This movement resembles an upward going staircase and matches the times when the US is switched again on after one pulsing period  $T_p$ . This is in line with the previous results from [24], which showed that the ARF-induced movement starts immediately as the US is switched on and stops as fast as it started when the US is switched off. No such staircase is visible for AS.

Additionally, for all positions  $\Delta y_i$  with a duty percentage of 50% and a pulse frequency of  $f_p = f_{\text{ex}}/10\,000$  the final measured value for AS is so low and close to zero that it might just be noise and no motion due to AS. On the other hand, the ARF data for the same data series shows a clear displacement of the particle. The reason that we measure for all positions  $\Delta y_i$  with 50% duty percentage and with a pulse frequency of  $f_p = f_{\text{ex}}/10\,000$  an AS-induced displacement is attributed to the slight differences in the experimental settings between BM series of different values of  $k$ .

Even though there are quantitative differences between the different pulse frequencies, qualitatively they have the same behavior. In all data series a reduced duty percentage is equivalent to a reduced and delayed buildup of the ARF and AS. Since lower duty percentages lead to less energy in the system, this behavior is expected. However, the reduction of the AS buildup is more than the reduction of the ARF. These different rates of reduction are more clearly visible in Fig. 11.

There the respective last normalized value of a data series of one specific duty percentage is plotted versus the duty

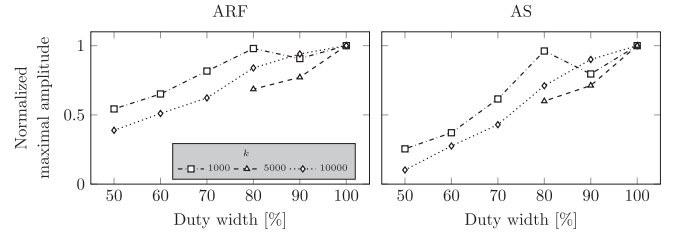


FIG. 11. Final normalized position at end of the buildup measurement of  $\Delta V_y$  (left column; ARF associated) and  $\Delta V_z$  (right column; AS associated) over duty percentage for the three pulsing frequencies  $f_p = f_{\text{ex}}/k$  and averaged over the three locations  $\Delta y_i = \{-0.06$  mm,  $-0.05$  mm,  $-0.04$  mm}. The outlier for  $k = 1000$  and 80% duty width is attributed to an unknown external disturbance within the OT laboratory.

percentage itself for each combination of BM point  $\Delta y_i$  and pulse frequency  $f_p$ . Each of these lines show a linear behavior over all duty percentages. However, the slope for the AS data is greater than for the ARF. This linear relation of the ARF for a one-dimensional standing pressure field to the acoustic energy density  $E_{\text{ac}}$  is in line with the theory

$$F_{\text{ARF}} \propto E_{\text{ac}} \propto p_a^2,$$

where  $p_a$  is the pressure of the acoustic field [6,7]. The same linear relation to the acoustic energy density ( $F_{\text{AS}} \propto E_{\text{ac}} \propto p_a^2$ ) is theoretically valid for AS [15] and also visible here. Nevertheless, the here depicted transient behavior of the ARF and AS suggests that the interrupted energy supply to the system causes an even further delay of the AS buildup compared to the ARF buildup. The generally lower values for the AS-induced displacement and also the later start of the AS buildup for  $f_p = f_{\text{ex}}/10\,000$  compared to  $f_p = f_{\text{ex}}/1000$  is attributed to the slight differences in the experimental settings and not a cause of the magnitude of  $f_p$  itself.

#### IV. CONCLUSION

We extended our previous OT setup to measure the effects of a pulsed ultrasonic excitation of a microacoustofluidic system on the buildup of AS and the ARF, and also on the final position of a microparticle because of AS and the ARF. We varied the pulse frequency  $f_p$  and duty width of the pulsed acoustic excitation to understand the effects of those parameters on the quantities of interest. In addition, we limited the difference of experimental settings between measurement series to a minimum for a valid comparison of the data. Our results show that the decrease in maximal displacement due to the ARF and the drag force from AS are both linear with respect to the applied duty percentage and more or less independent of the pulse frequency  $f_p$ . However, the decrease of AS with lower duty percentage is for all BMs faster than for the ARF. Even though our BM time span is limited to 120 000 acoustic excitation periods  $1/f_{\text{ex}}$  ( $\approx 96$  ms), we still manage to observe a significant level of streaming suppression, confirming the experimental results of Hoyos and Castro [12,13], and laying grounds for new theoretical studies that might improve our understanding of the AS buildup.

- [1] C. Eckart, *Phys. Rev.* **73**, 68 (1948).
- [2] W. L. M. Nyborg, *Phys. Acoustics* **2**, 265 (1965).
- [3] H. Schlichting, *Phys. Z.* **33**, 327 (1932).
- [4] T. Baasch, A. Pavlic, and J. Dual, *Phys. Rev. E* **100**, 061102(R) (2019).
- [5] K. Yosioka and Y. Kawasima, *Acta Acust. Acust.* **5**, 167 (1955).
- [6] H. Bruus, *Lab Chip* **12**, 1014 (2012).
- [7] L. Gor'kov, *Sov. Phys. Dok.* **6**, 773 (1962).
- [8] L. V. King, *Proc. R. Soc. A* **147**, 212 (1934).
- [9] R. Barnkob, P. Augustsson, T. Laurell, and H. Bruus, *Phys. Rev. E* **86**, 056307 (2012).
- [10] D. Van Assche, E. Reithuber, W. Qiu, T. Laurell, B. Henriques-Normark, P. Mellroth, P. Ohlsson, and P. Augustsson, *Sci. Rep.* **10**, 3670 (2020).
- [11] M. Antfolk, P. B. Muller, P. Augustsson, H. Bruus, and T. Laurell, *Lab Chip* **14**, 2791 (2014).
- [12] M. Hoyos and A. Castro, *Ultrasonics* **53**, 70 (2013).
- [13] A. Castro and M. Hoyos, *Ultrasonics* **66**, 166 (2016).
- [14] J. T. Karlsen, W. Qiu, P. Augustsson, and H. Bruus, *Phys. Rev. Lett.* **120**, 054501 (2018).
- [15] J. S. Bach and H. Bruus, *Phys. Rev. Lett.* **124**, 214501 (2020).
- [16] B. G. Winkelmann and H. Bruus, *J. Acoust. Soc. Am.* **149**, 3917 (2021).
- [17] G. Thalhammer, R. Steiger, M. Meinschad, M. Hill, S. Bernet, and M. Ritsch-Marte, *Biomed. Opt. Express* **2**, 2859 (2011).
- [18] P. G. Bassindale, D. B. Phillips, A. C. Barnes, and B. W. Drinkwater, *Appl. Phys. Lett.* **104**, 163504 (2014).
- [19] C. Fury, P. H. Jones, and G. Memoli, in *Proceedings of the SPIE, Optical Trapping and Optical Micromanipulation XI* Vol. 9164, edited by K. Dholakia and G. C. Spalding (SPIE, 2014).
- [20] S. Lakämper, A. Lamprecht, I. A. T. Schaap, and J. Dual, *Lab Chip* **15**, 290 (2015).
- [21] A. Lamprecht, S. Lakämper, T. Baasch, I. A. T. Schaap, and J. Dual, *Lab Chip* **16**, 2682 (2016).
- [22] G. Thalhammer, C. McDougall, M. P. MacDonald, and M. Ritsch-Marte, *Lab Chip* **16**, 1523 (2016).
- [23] A. Lamprecht, C. Goering, I. A. T. Schaap, and J. Dual, *J. Micromech. Microeng.* **31**, 034004 (2021).
- [24] C. Goering and J. Dual, *Phys. Rev. E* **104**, 025104 (2021).
- [25] P. B. Muller and H. Bruus, *Phys. Rev. E* **92**, 063018 (2015).
- [26] P. Hahn, A. Lamprecht, and J. Dual, *Lab Chip* **16**, 4581 (2016).